Consequences of Using Different Altimeter Products on the Interpretation of the Sea Level Change 1993-2001

M. Wenzel and J. Schröter

Alfred Wegener Institute for Polar and Marine Research, Bremerhaven, Germany
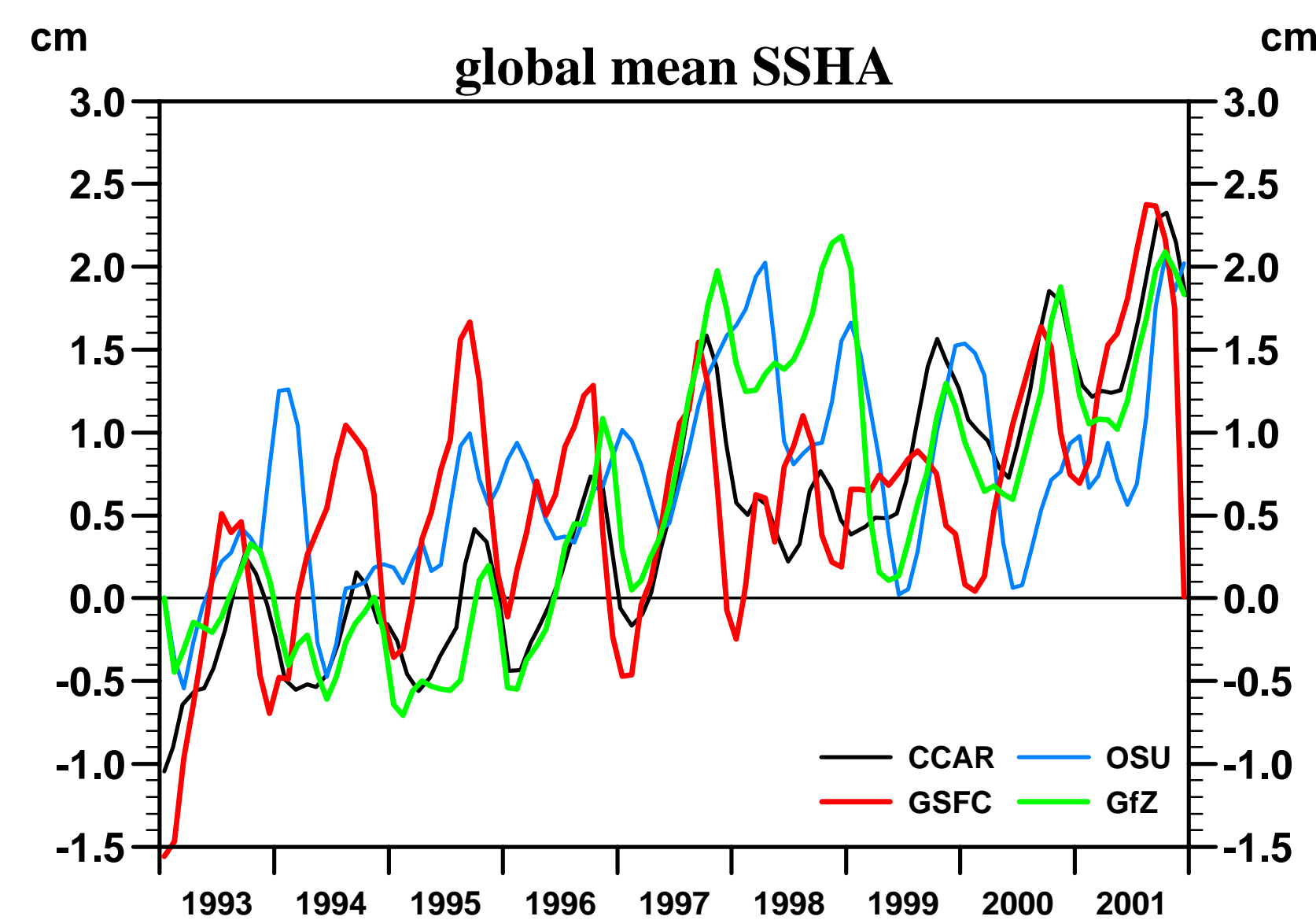
Introduction

Fig. 1: Evolution of the global mean sea level during 1993-2001 as estimated by four different groups processing the TOPEX/Poseidon altimeter measurements.
Data provided by
CCAR: Colorado Center for Astrodynamics Research (Eric Leuliette)
OSU : Ohio State University (Chung-Yen Kuo)
GSFC: NASA/GSFC Ocean Pathfinder Project (ftp server)
GfZ : Geoforschungszentrum Potsdam (Saskia Esselborn)

In principle sea level changes can be measured accurately by satellite altimetry, but the processing of the data includes many corrections. At this step the choise of the algorithms and the additional correction data is free to subjective preferences to a certain extent. For sure each choise has its own justification, but this finally leads to differences in the products that are delivered to the end user. As an example **Fig.1** shows the temporal evolution of the global mean sea level as estimated by four different groups.

From the end users point of view it is interesting to see what are the consequences of using different products e.g. in ocean state estimation. For that reason we performed two assimilation experiments utilizing the sea level anomaly maps from the NASA/GSFC Ocean Pathfinder Project (**NASA/GSFC**) and from the Geoforschungszentrum Potsdam (**GfZ**) respectively covering the years 1993 to 2001.

assimilation experiment	SSHA data source
BRIO2C	NASA/GSFC
B2ntp	GfZ Potsdam

Both assimilation experiments, **BRIO2C** and **B2ntp**, start from the same first guess. Thus they differ only in the sea surface height anomalies used!

Method

The OGCM that is used to study the impact of the different sea level anomaly products on the ocean state is based on the Hamburg Large Scale Geostrophic model LSG. The main improvement of the model is the ability to estimate the single contributions to sea level change, the steric (thermosteric, halosteric) and the non-steric effects (local freshwater balance, mass redistribution) seperately.

The model has a $2^o \times 2^o$ horizontal resolution, 23 vertical layers and a ten day timestep. Nine years (1993-2001) of respective TOPEX/Poseidon (T/P) sea surface height anomalies are assimilated into the model. In addition the SHOM98.2 mean sea surface relative to the GRACE geoid (GfZ) as well as sea surface temperatures and ice cover information from Reynolds (2002) are assimilated into the model. Furthermore background information from the Levitus WOA98 is used.

To adjust the model to the data the adjoint method is employed. The control parameters of this optimization are the models initial temperature and salinity state as well as the forcing fields (windstress, air temperature and surface freshwater flux). The forcing is optimized via an empirical orthogonal function (EOF) decomposition, with the first guess taken from the NCEP reanalysis.

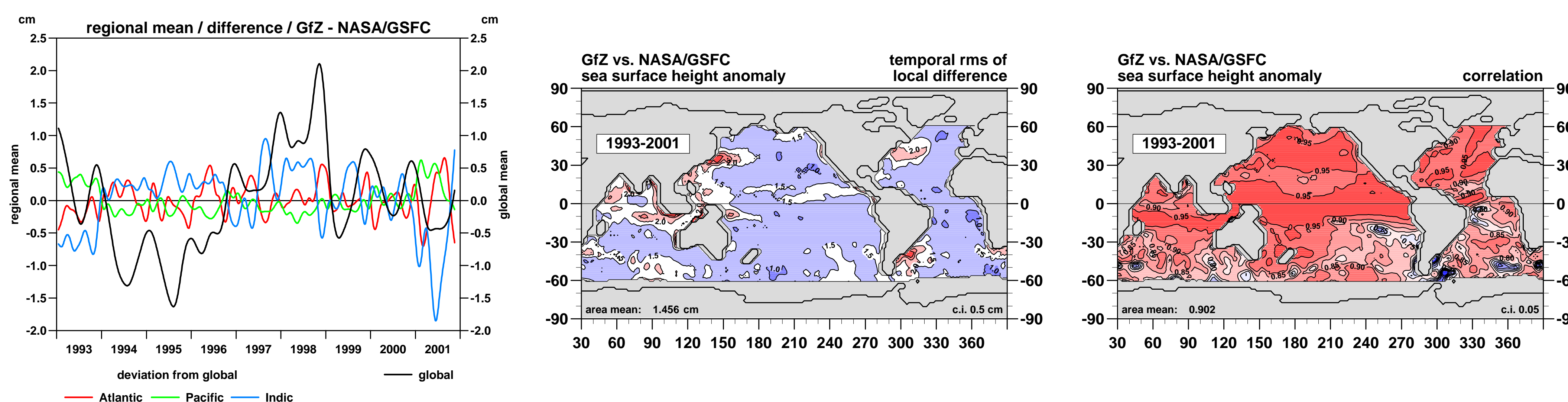## Comparing TOPEX Data Products: GfZ vs. NASA/GSFC

Fig. 2: (left) Temporal evolution of area mean differences between the **NASA/GSFC** and the **GfZ** dataset. For the single oceans only the excess to the global difference is shown! (center) Temporal RMS of the local differences and (right) the local correlation
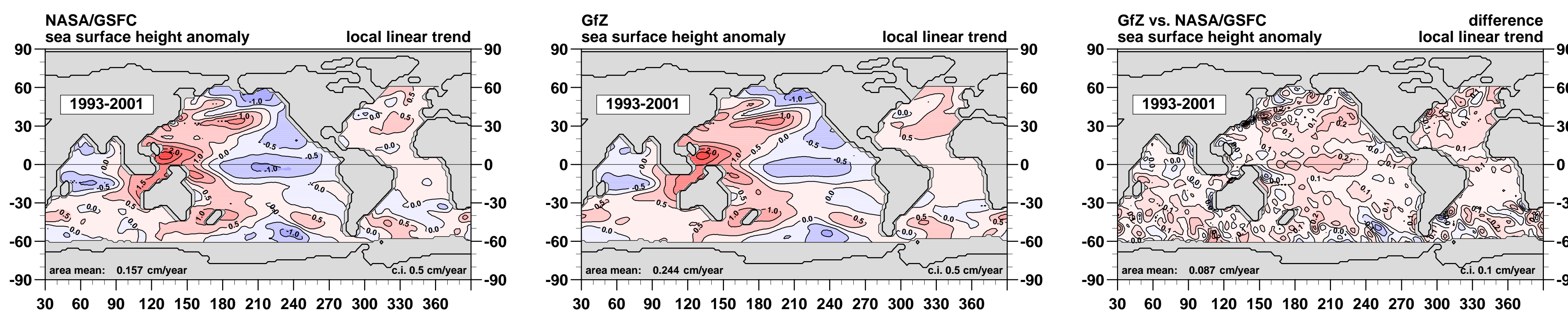

Fig. 3: Local sea level trend as derived from the **NASA/GSFC** dataset (left) and from the **GfZ** dataset (center) as well as the difference in these trends (right)

It is not the purpose of this presentation to compare or even judge the single correction steps applied to the TOPEX data by the different groups. Therefore we only give a short comparison of the finally resulting products used in the assimilation experiments.

Although the datasets from the **NASA/GSFC** and from the **GfZ** respectively, are hightly correlated in time (**Fig.2 right**), especially in the northern hemispere, one finds differences in the temporal evolution of the global mean, which range up to ±2cm (**Fig.2 left**). Even for the area mean of the single ocean basins one finds additional deviations exceeding the global up to ±1.5cm. Nevertheless the temporal RMS of the differences show up fairly constant at a 1cm level (**Fig.2 center**) with maximum values (up to 3cm) found in regions with hight oceanic variability like in the Kuroshio, at the Falkland/Malvinas Plateau or in the Gulf Stream area.

The local linear trend of the **NASA/GSFC** (**Fig.3 left**) and the **GfZ** dataset (**Fig.3 center**) exhibit essentially the same spatial structure but with an 0.087cm/year global mean offset. The positive differences in the trend range up to 0.3cm/year locally, e.g. in the North Pacific, but especially in the region south of 30ºS one finds also negative differences up to –0.2cm/year (**Fig.3 right**).

Comparing Model Sea Surface Height to Data

Figure 4 shows that the optimized models reproduce their corresponding global mean sea level data well. This is true especially for the interannual variabilty, while the amplitude of the annual cycle is underestimated by the models. The latter appears to be a general deficit of the OGCM used and leads to the maxima in the temporal RMS differences shown in **Fig.5**. The spatial distribution of the RMS is very simular for both experiments and reaches values of up to 7cm especially in the tropics and in the western boundary currents. Also their global mean RMS values, which are the measure of success in the assimilation, appear to be comparable (2.83cm and 2.81cm respectively).

The same good correspondence between the two experiments one also finds for the differences between the modeled temporal mean sea level and the **SHOM98.2** sea level (**Fig.6**). In most of the world ocean the differences are below 10cm. Larger values are found only in the circum polar belt, where the model produces a much broader Circum Polar current than expected from the data. The same holds for the western boundary currents, while the strong deviations near the Indoneasian Throughflow and in the Carribic may be explained by de-

ficits in the geoid. The spatial RMS value of these difference fields are again comparable (10.58cm and 10.84cm respectively)

The strong similarity in the fit of the model to the data encourages to look at the effect of the difference in the data on the ocean state.
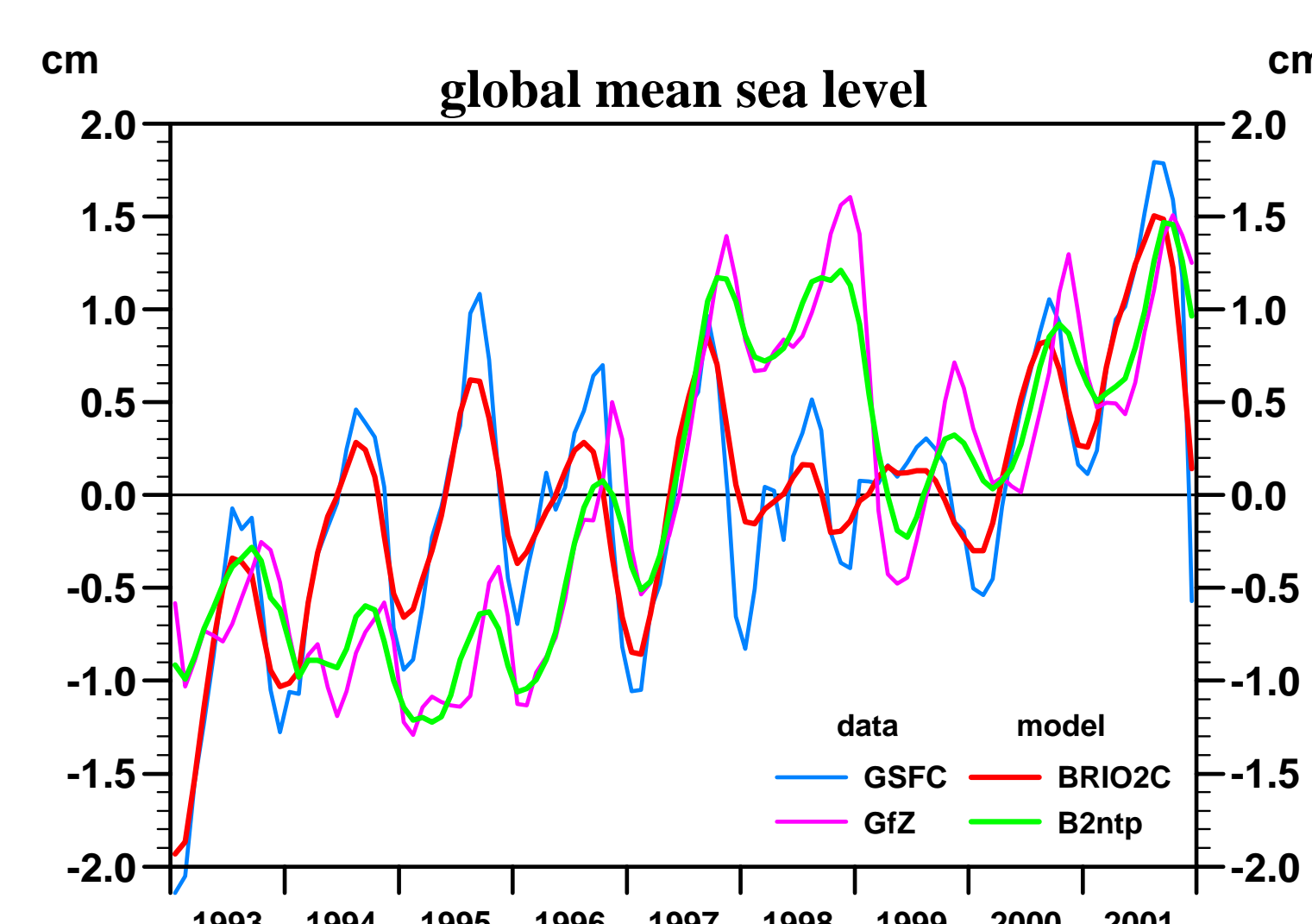

Fig. 4: Global mean sea level anomaly from the two assimilation experiments, **BRIO2C** and **B2ntp**, as compared to the corresponding data
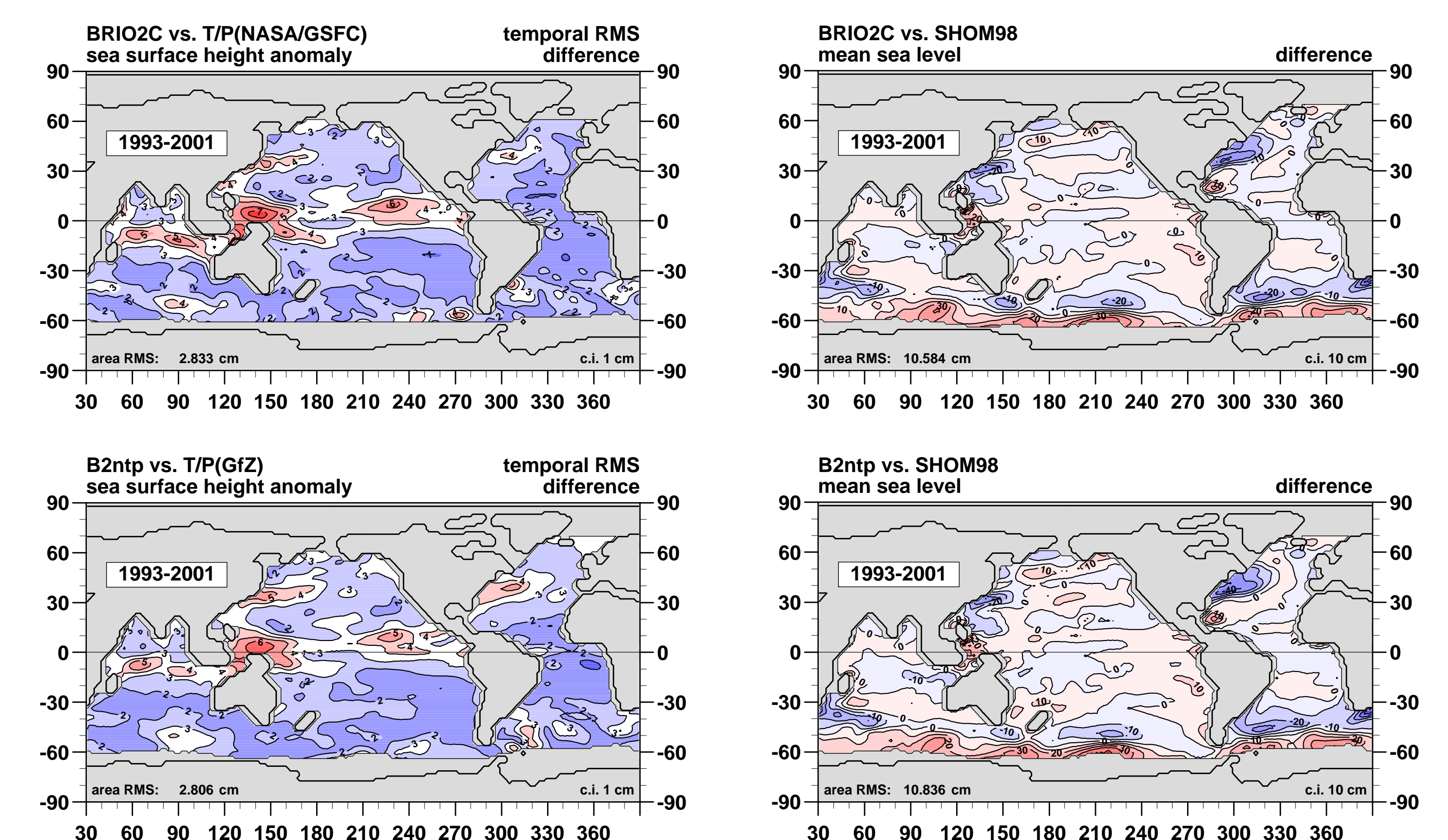

Fig. 5: Local temporal RMS of the modeled SSHA difference between model and corresponding data, for experiment **BRIO2C** (top) and **B2ntp** (bottom).

Fig. 6: Temporal mean sea level for the assimilation experiments **BRIO2C** (top) and **B2ntp** (bottom) compared to the **SHOM98.2** mean sea surface height referenced to the GRACE geoid
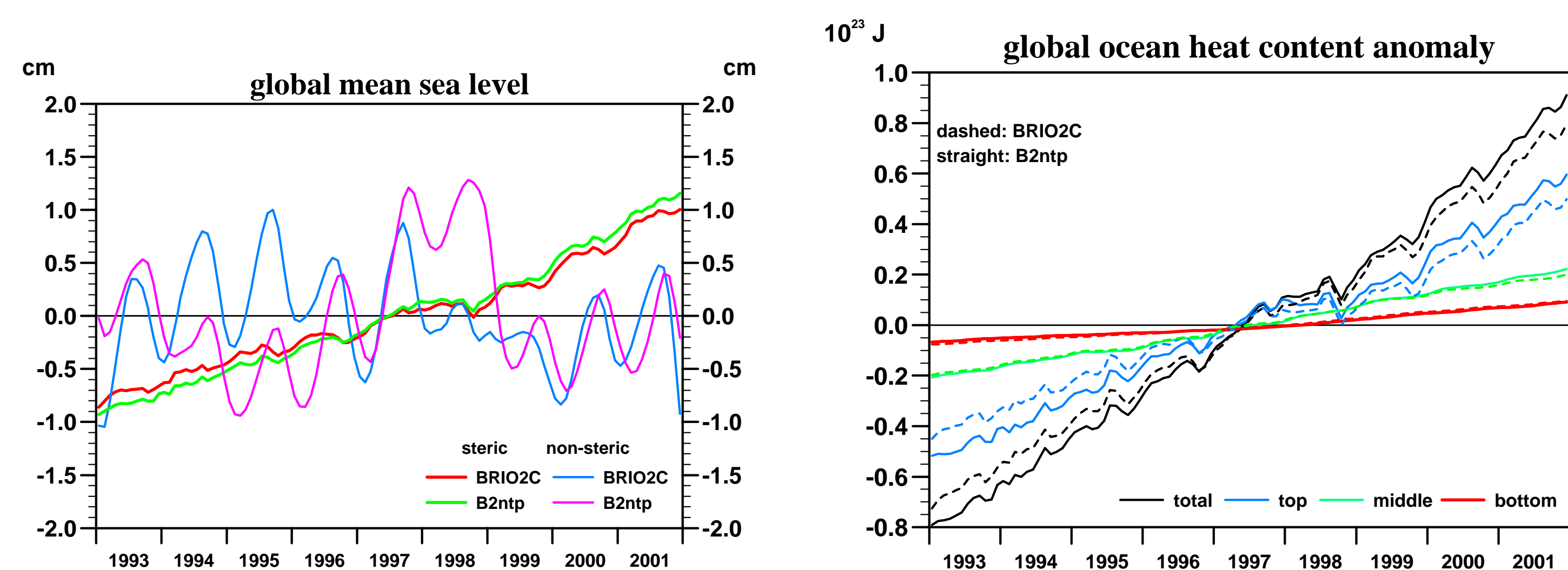
Comparing Model Sea Surface Height

Fig. 7a: Decomposition of the temporal evolution of global mean sea level into steric and non-steric part for the model solutions **BRIO2C** and **B2ntp**.
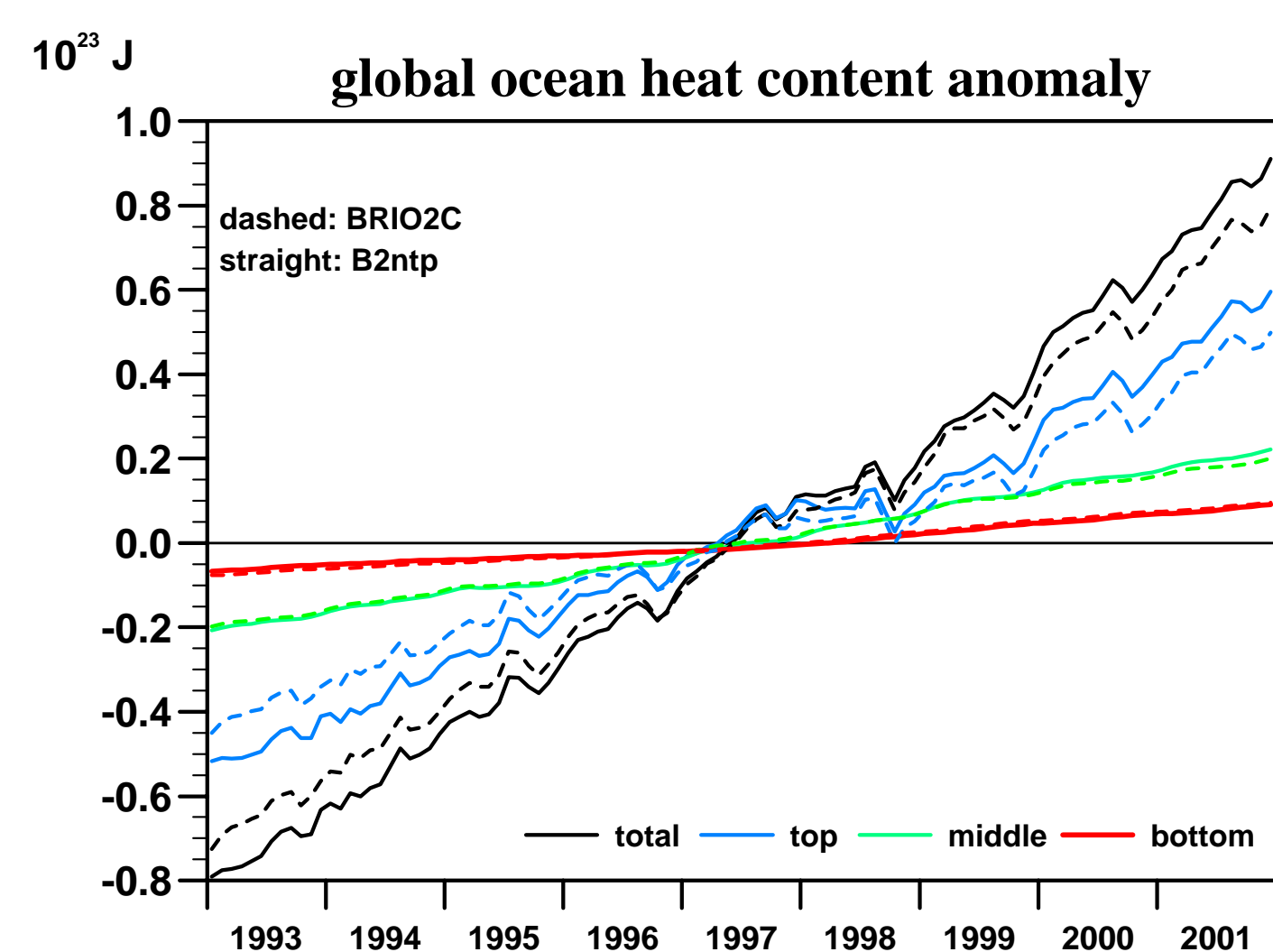

Fig. 7b: Corresponding global ocean heat content anomaly for the depth ranges: total=[ζ-bottom], top=[ζ-512m], middle=[512m-2250m] and bottom=[2250m-bottom]

For both experiments, **BRIO2C** and **B2ntp** respectively, the main contribution to global sea level rise is given by the linear trend of the (thermo-)steric component, which is slightly higher using the **GfZ** data (experiment **B2ntp**) than in the results obtained when utilizing the **NASA/GSFC** data. The main differences in the mean sea level is explained by the non-steric component, which reflects the annual to interannual variability (**Fig.7a**).

Only about 60% of the thermosteric sea level rise originates from the upper 512m of the ocean. Thus the thermal trend in the deeper layers contribute an essential part (**Fig.7b**).

Figure 8a shows the local sea level trends resulting from the two models **BRIO2C** and **B2ntp** that should be compared to the corresponding data shown in **Fig.3**. Decomposing the sea level trends into its thermosteric, halosteric and non-steric components (**Fig.8b-d**) shows that even on local scale the main contribution to sea level change is given by the thermosteric part. But the halosteric one cannot be neglected! There are large regions where it is of the same size as the thermosteric.

Differences between the models appear mainly in the non-steric part of the trends. In contrast to the differences in the corresponding data trends **Fig.3 right** these differences are of opposite sign in the North and the South Pacific. In the thermosteric as well as in the halosteric part differences are found mainly in the Atlantic and in the circumpolar belt.
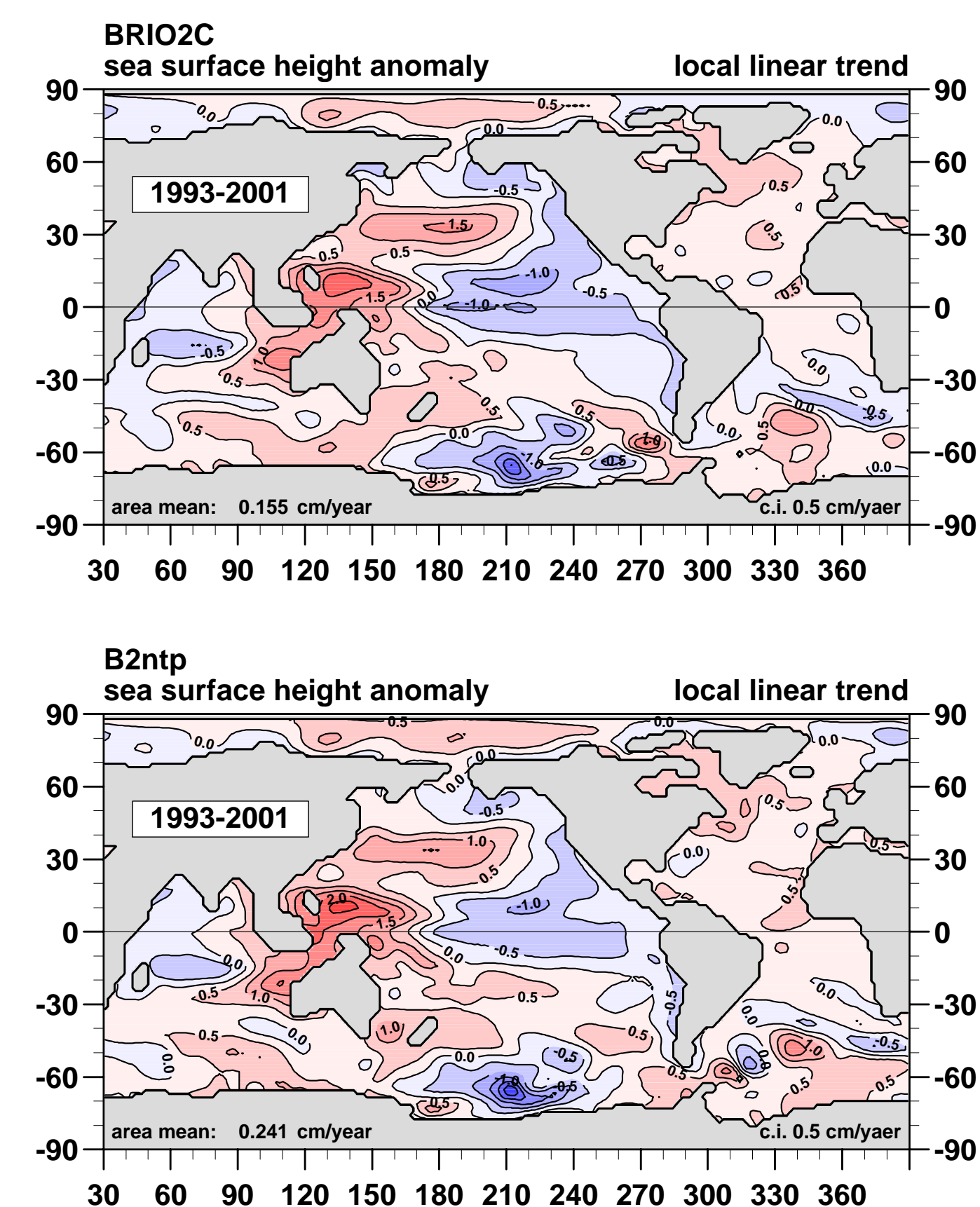

Fig. 8a: Local sea level trend of the model solutions **BRIO2C** (upper row) and **B2ntp** (lower row). REMARK: The area mean values are given for the data covered area (see e.g. **Fig.3**)
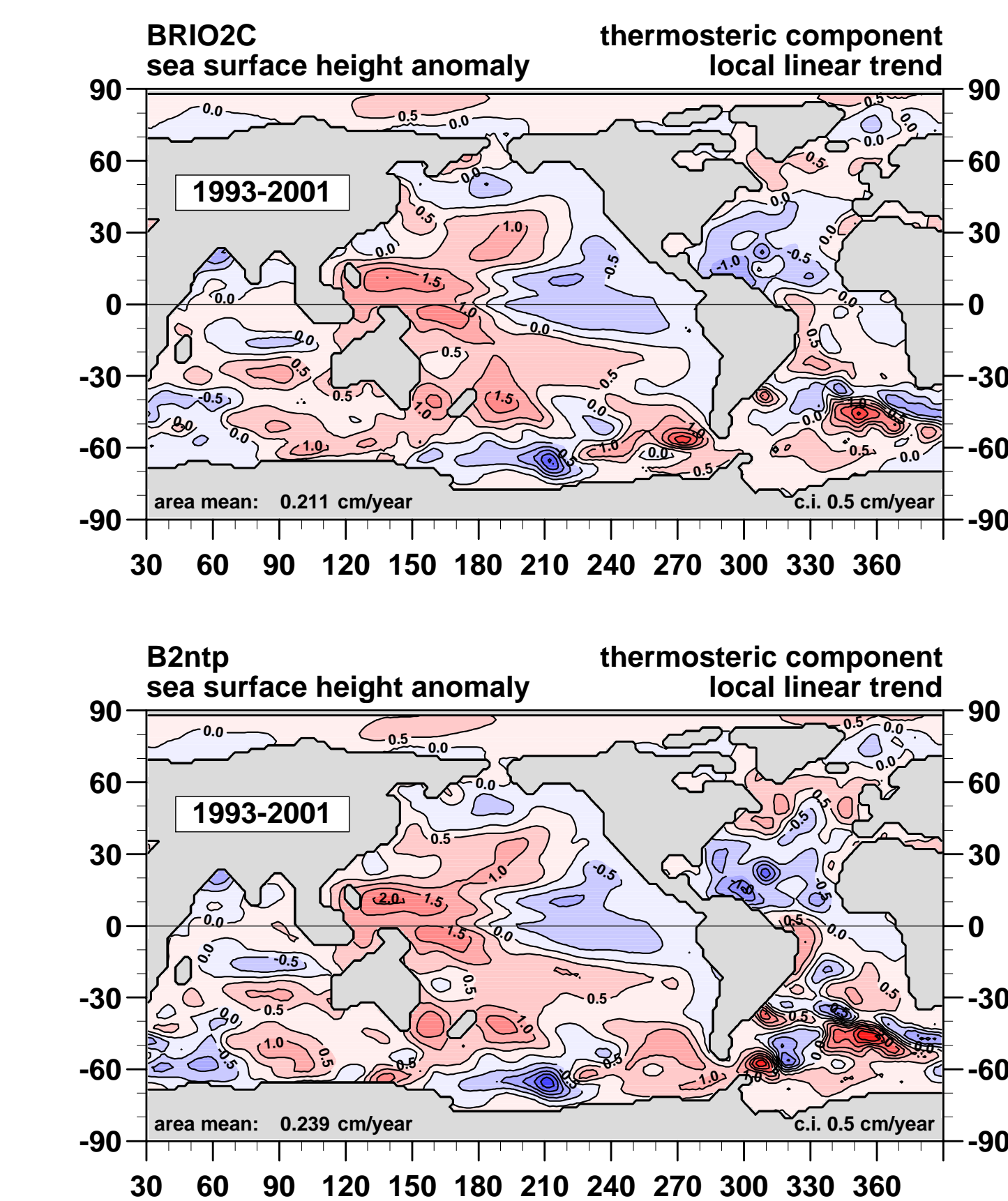

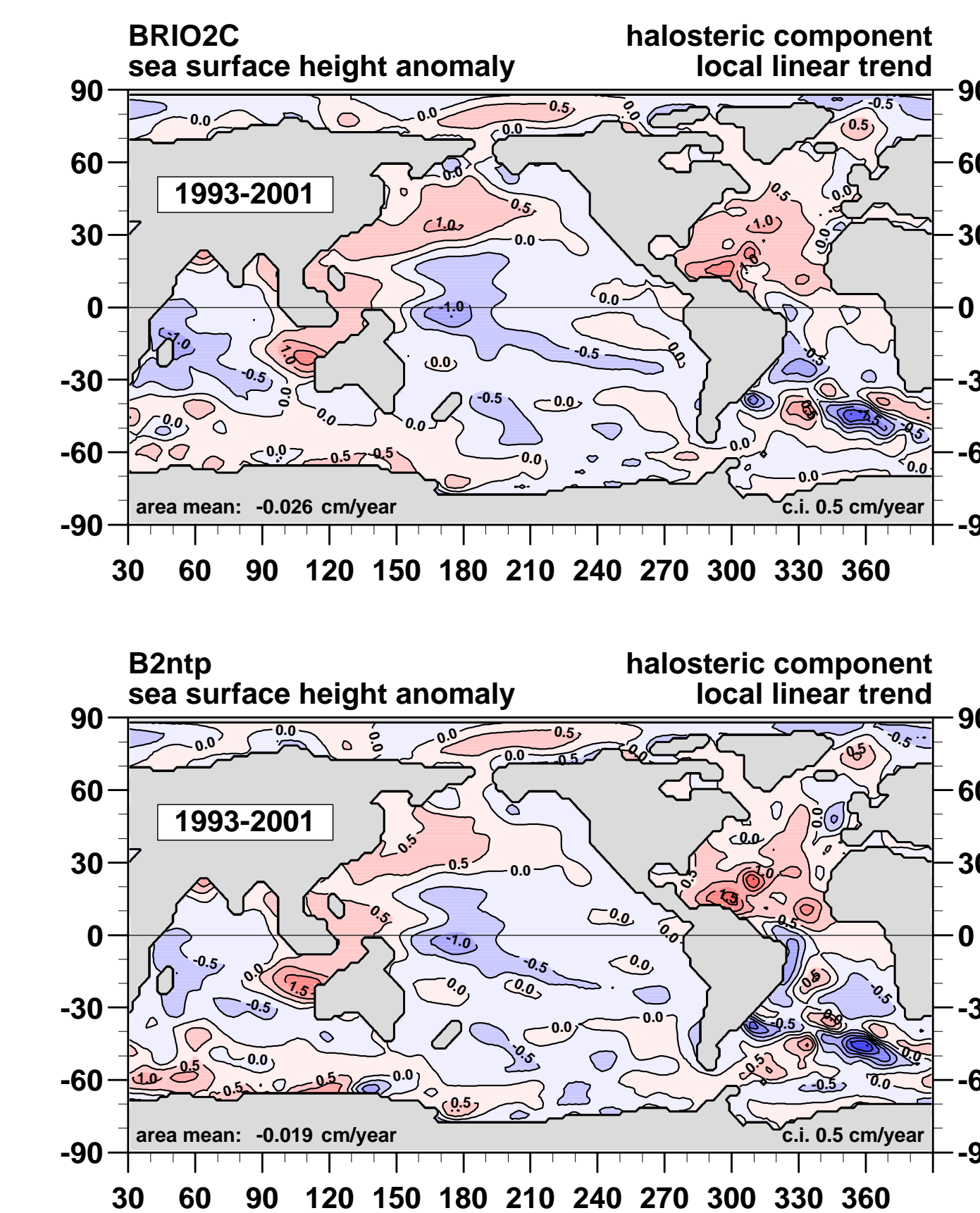**Fig. 8b:** same as **Fig. 8a:** but for the thermosteric component

Fig. 8c: same as **Fig. 8a:** but for the halosteric component
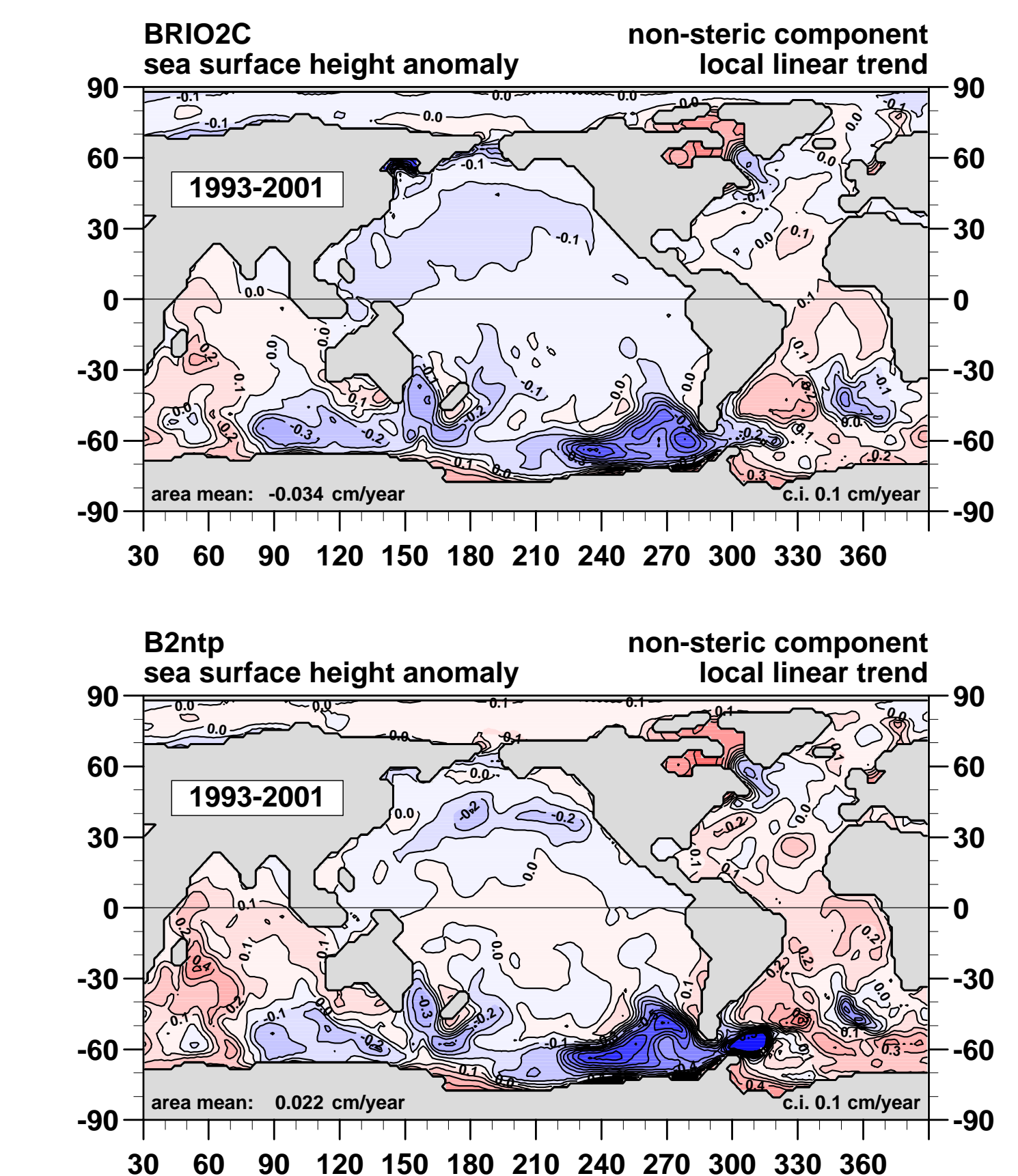

Fig. 8d: same as **Fig. 8a:** but for the non-steric component
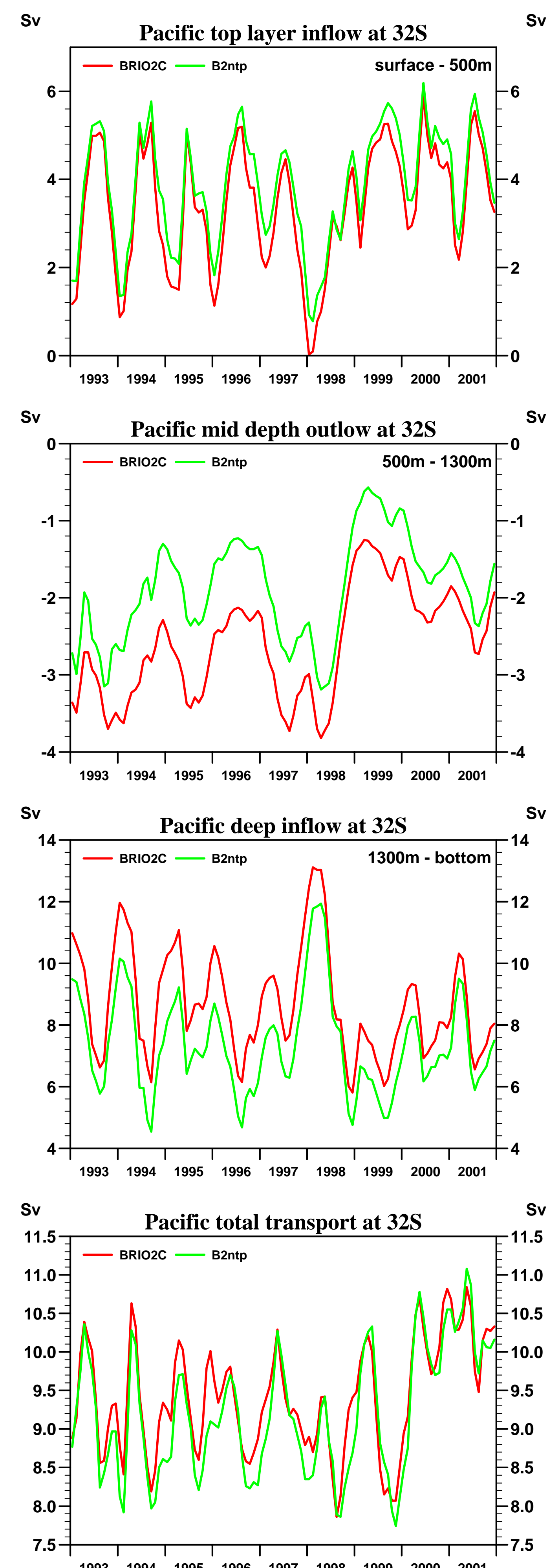
Pacific Circulation

Fig. 9: Pacific mass transport across 32ºS for the depth ranges (topmost to undermost): [ζ-500m], [500m-1300m], [1300m-bottom] and [ζ-bottom]
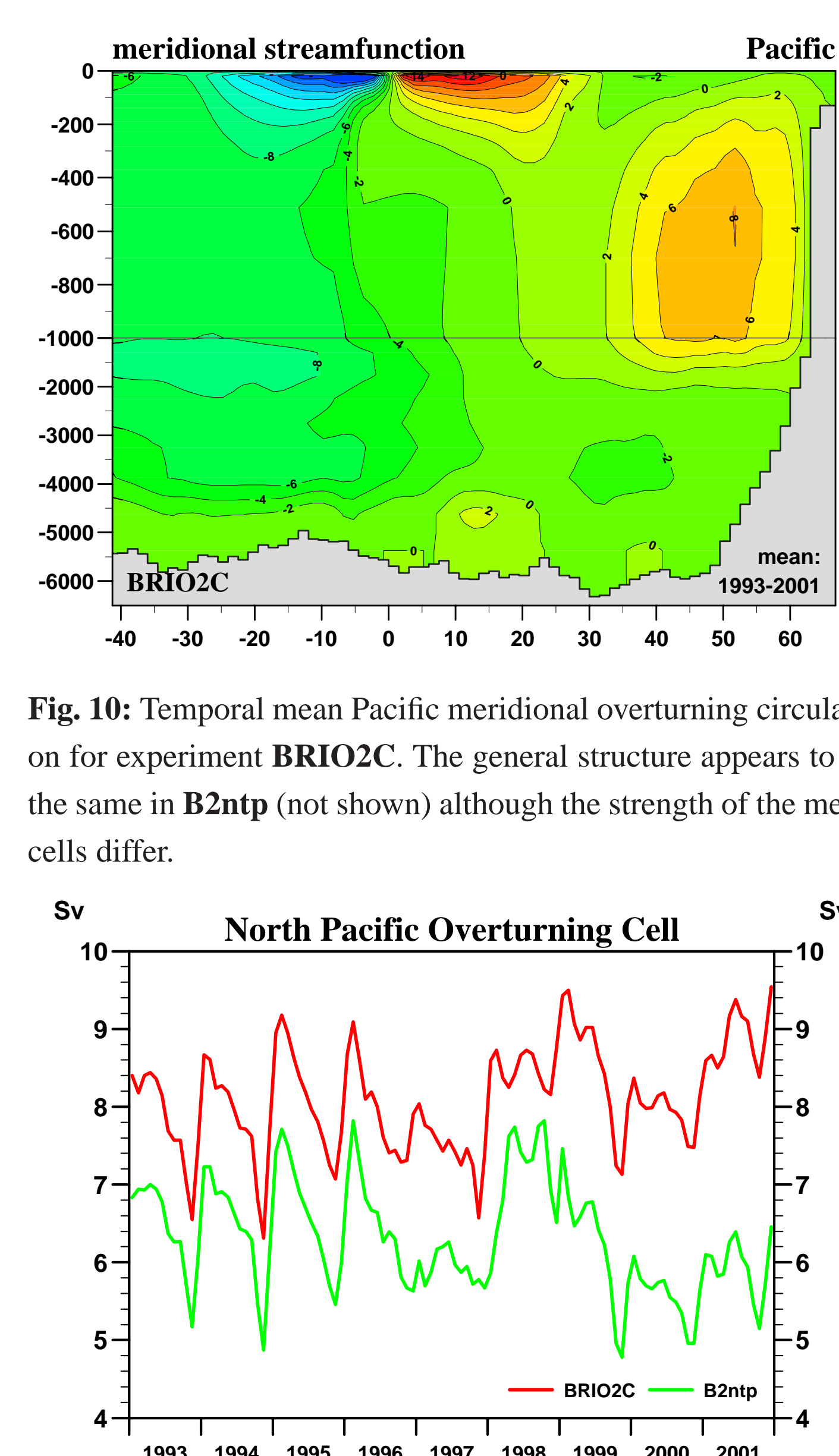

Fig. 10: Temporal mean Pacific meridional overturning circulation for experiment **BRIO2C**. The general structure appears to be the same in **B2ntp** (not shown) although the strength of the mean cells differ.

Fig. 11: Temporal variations in the strength of the North Pacific overturning cell for both experiments, **BRIO2C** and **B2ntp**.

The differences in the sea level variations influence the oceanic circulation as demonstrated here by the Pacific overturning. Although the total transport across 32ºS (**Fig.9**) appears to be nearly the same for both experiments, **BRIO2C** and **B2ntp** respectively, one finds differences of up to two Sverdrup especially in the deep inflow and in the mid-depth outflow which are reciprocally compensating.

This difference is not that pronounced in the general structure of the overturning (**Fig.10**) but in its strength. As an example **Fig.11** compares the strength of the northern cell centered at about 50ºN and 500m depth. This overturning cell shows nearly the same temporal behaviour for **BRIO2C** and **B2ntp** on short timescales, but it also exhibits different trends especially after the 1997 El Niño event.

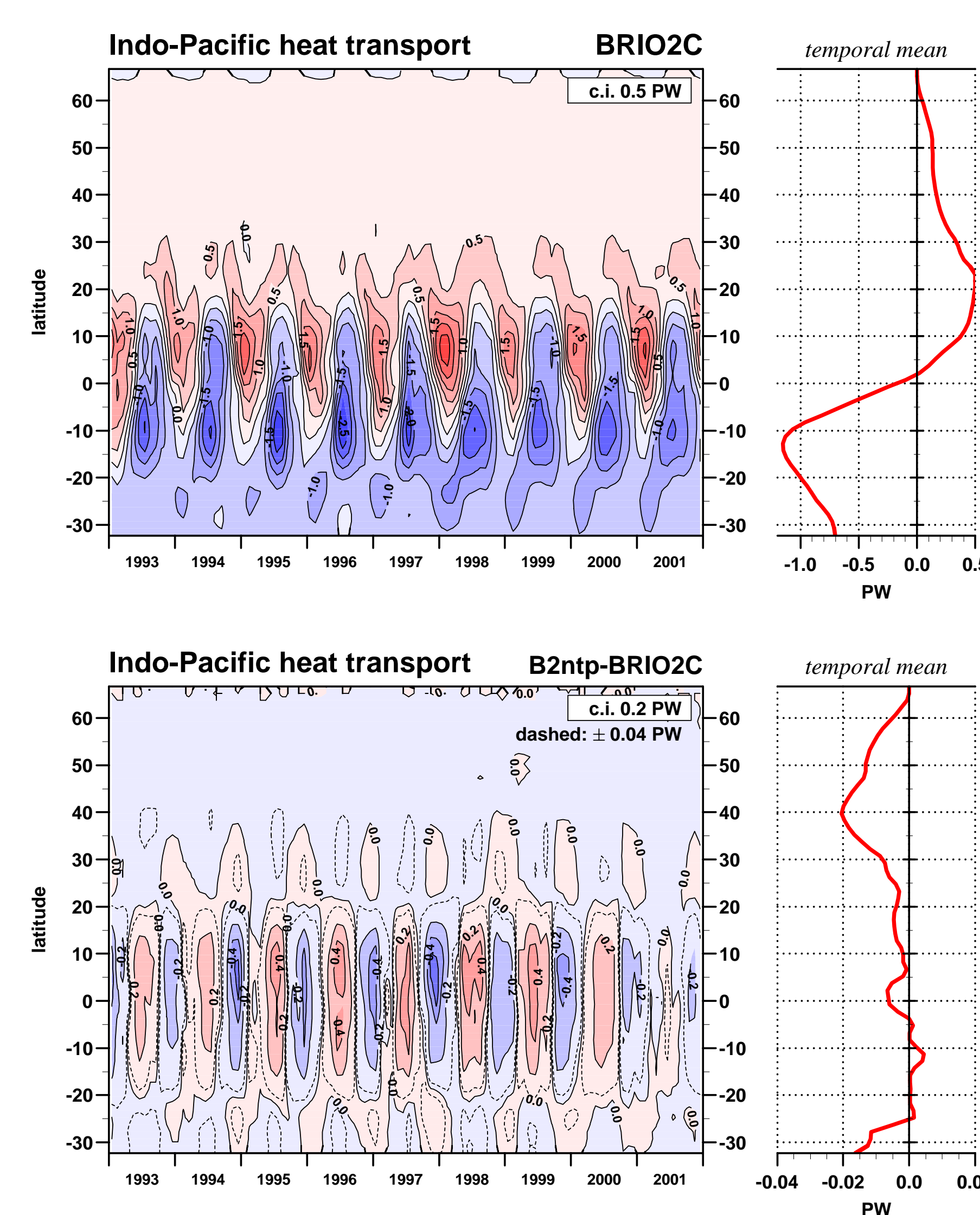# Indo-Pacific Heat Transport

Fig. 12: Meridional heat transport in the Indo-Pacific Ocean for experiments **BRIO2C** (top) and the difference between the two model results, **B2ntp** minus **BRIO2C** (below).

The meridional heat transport in the two model solutions, **BRIO2C** and **B2ntp** respectively, differ mainly in the equatorial belt between 5ºS and 15ºN. Only the transport in the Indo-Pacific is shown here, but this holds for all of the global ocean. The differences mainly appear in the amplitude of the annual cycle which is altered by about 0.5PW, while the temporal means, given in the right graphs of **Fig.12**, stay approximately the same. Outside the equatorial band the differences stay well below 0.04PW as indicated by the additional dashed lines in the lower left plot.

Summary

- The sea level anomalies, as derived by different groups from the TOPEX/Poseidon altimeter measurements exhibit strong differences related to the respective correction algorithms / data chosen.

- The ocean model can be fitted to the different datasets with equal quality

- The assimilated model solutions exhibit equal steric contributions to sea level change. The differences in the datasets are mainly reflected in the non-steric part.

- Nevertheless the differences in the sea level datasets project into the oceanic circulation. This can be seen especially in the mass transports, while for the heat transports essential differces are found only in the equatorial belt (5ºS - 15ºN) in the amplitude of the annual cycle.

Corresponding e-mail adresses:
mwenzel@awi-bremerhaven.de   jschroeter@awi-bremerhaven.de